



HAL
open science

Noble Metal Nanocluster Formation in Epitaxial Perovskite Thin Films

Mihee Lee, Rémi Arras, Ryota Takahashi, Bénédicte Warot-Fonrose, Hiroshi Daimon, Marie-José Casanove, Mikk Lippmaa

► **To cite this version:**

Mihee Lee, Rémi Arras, Ryota Takahashi, Bénédicte Warot-Fonrose, Hiroshi Daimon, et al.. Noble Metal Nanocluster Formation in Epitaxial Perovskite Thin Films. ACS Omega, 2018, 3 (2), pp.2169 - 2173. 10.1021/acsomega.7b02071 . hal-01735718

HAL Id: hal-01735718

<https://hal.science/hal-01735718>

Submitted on 24 Jun 2019

HAL is a multi-disciplinary open access archive for the deposit and dissemination of scientific research documents, whether they are published or not. The documents may come from teaching and research institutions in France or abroad, or from public or private research centers.

L'archive ouverte pluridisciplinaire **HAL**, est destinée au dépôt et à la diffusion de documents scientifiques de niveau recherche, publiés ou non, émanant des établissements d'enseignement et de recherche français ou étrangers, des laboratoires publics ou privés.

Noble Metal Nanocluster Formation in Epitaxial Perovskite Thin Films

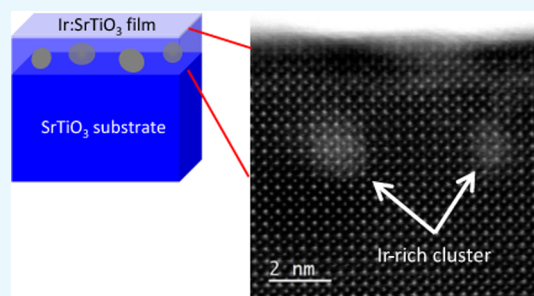
Mihee Lee,^{*,†,‡,§} Rémi Arras,[‡] Ryota Takahashi,[§] Bénédicte Warot-Fonrose,[‡] Hiroshi Daimon,[†] Marie-José Casanove,[‡] and Mikk Lippmaa^{*,§}

[†]Graduate School of Materials Science, Nara Institute of Science and Technology (NAIST), 8916-5 Takayama, Ikoma, Nara 630-0192, Japan

[‡]Centre d'Elaboration des Matériaux et d'Etudes Structurales (CEMES), CNRS UPR 8011 and Université de Toulouse, 29 rue Jeanne Marvig, Toulouse F-31055, France

[§]Institute for Solid State Physics, The University of Tokyo, 5-1-5 Kashiwanoha, Kashiwa 277-8581, Japan

ABSTRACT: We studied the synthesis of nanocomposite materials consisting of noble metal clusters embedded in an oxide semiconductor matrix. The embedded nanostructures form in a simple self-organized single-step growth process. The primary interest is in developing materials for photo-electrochemical energy conversion where spatially inhomogeneous band structures can enhance photogenerated charge separation and carrier extraction from a semiconductor. We show that spontaneous segregation of metallic Ir occurs during the initial growth of an Ir:SrTiO₃ thin film. Cross-sectional transmission electron microscopy suggests that the nanoscale Ir clusters are epitaxial with the host lattice, and their presence is not detectable by surface morphology measurements.



1. INTRODUCTION

Composite materials consisting of an oxide matrix combined with metal nanostructures are widely studied in the area of catalysis for pollution control¹ and energy conversion.² The most common composite designs consist of nanoscale metal particles deposited on a ceramic oxide support, which typically has a passive role and only serves to provide a thermally and mechanically stable substrate with a large surface area for the catalytically active metal nanoparticles.³ A different class of nanocomposites involves metal nanoparticles either at the surface of or embedded in an oxide support where the interplay between the oxide support and the metal leads to the desired catalytic functionality. Plasmonic energy-harvesting photocatalysts are an example of this class of materials.⁴ Another well-known example is the use of noble metal cocatalysts on the surface of photocatalytic semiconductor oxides for efficient extraction of photogenerated holes or electrons.⁵

Bulk nanoscale metal–oxide composites, where metal nanoparticles are embedded in an oxide matrix, are less common, but a photo-electrochemical water splitting electrode based on self-organized Ir metal pillars in a SrTiO₃ matrix has recently been reported.⁶ Spontaneous Ir metal segregation was suggested to occur at the initial substrate interface during Ir-doped SrTiO₃ growth, which eventually leads to the formation of macroscopic metal pillars along the film growth direction. A slightly similar idea has been used to design an intelligent Pd catalyst for automotive emission control.⁷

From the point of view of photocatalytic energy conversion, bulk metal–oxide composites have a number of advantages.

Because the embedded nanostructures form in a self-organized process, the composite material can be grown in a relatively simple and cheap single-step synthesis process without the need for nanoscale patterning.⁸ Compared to various three-dimensional nanostructures grown on the surface of a catalyst,⁹ nanostructures embedded in the crystal lattice of an oxide matrix are mechanically robust, which may extend the working life of a practical photocatalyst. Composites containing nanoscale noble metal inclusions close to the surface of a semiconductor matrix are of particular interest because, because of the large work function of noble metals, it is possible to induce local changes in the surface band bending of the semiconductor, similar to cocatalysts precipitated on surfaces.¹⁰ In an electronic sense, a thin nanocomposite layer is thus equivalent to a semiconductor photoelectrode coated with noble metal cocatalyst nanoparticles but offers a more stable mechanical structure with better control over the spatial variation of the electronic structure in the vicinity of the noble metal inclusions.

In general, the three-dimensional morphology of nanoscale inclusions can be controlled during thin film deposition by lattice strain, growth rate, growth temperature, and the oxygen pressure. The oxygen pressure is a particularly important process parameter for noble metal dopants such as Ir. At relatively high pressures, in the range of 10⁻¹ Torr, Ir can be

Received: December 27, 2017

Accepted: February 13, 2018

Published: February 21, 2018

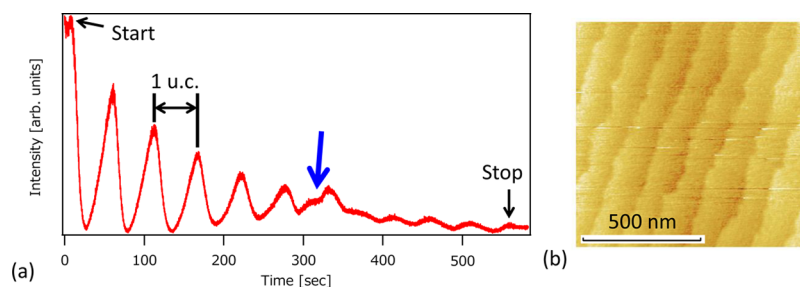


Figure 1. RHEED oscillation and sample surface morphology. (a) RHEED specular spot intensity oscillation observed during film deposition. A change in the surface termination occurs after the growth of five u.c., marked by an arrow. (b) AFM surface morphology of a 4 u.c. thick Ir(5%):SrTiO₃ film grown on a SrTiO₃(001) substrate. The heights of all step edges are ~ 0.4 nm.

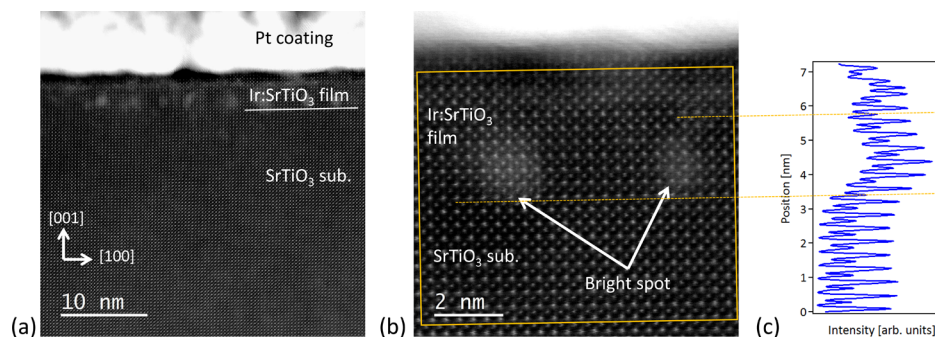


Figure 2. Cross-sectional HAADF-STEM image of a 5% Ir-doped SrTiO₃ (10 u.c.) film on a SrTiO₃ (001) substrate. (a) Wide view and (b) magnified view of the film observed along the [010] zone axis. (c) HAADF intensity profile in the marked square region integrated along the horizontal direction (parallel to the substrate interface).

oxidized to IrO₃, which is volatile, and Ir is thus lost during film growth to evaporation.¹¹ At intermediate oxygen pressures of 10⁻³ to 10⁻² Torr, earlier work has shown the occurrence of macroscopic metal segregation for several noble metals.⁶ The same work suggested, on the basis of atomic force microscopy (AFM) observations, that films grown at low pressures of around 10⁻⁶ Torr appear to be homogeneous. It is thus interesting to look at the Ir dopant behavior in this lower oxygen pressure regime to determine if Ir dopants are indeed homogeneously distributed in the host lattice or some form of nanoscale clustering still occurs.

In this work, we therefore study the surface morphology, growth mode, and Ir dopant distribution in films grown at an oxygen pressure of 10⁻⁶ Torr. The Ir doping was set at a level of 5%, which is a typical doping level for dopants in SrTiO₃-based photocatalyst studies.¹² We show that despite having apparently smooth step-and-terrace surfaces, the Ir:SrTiO₃ films grown under these conditions exhibit nanoscale Ir segregation.

2. EXPERIMENTAL AND CALCULATION DETAILS

Ir-doped SrTiO₃ thin films were grown on TiO₂-terminated SrTiO₃(001) substrates by pulsed laser deposition (PLD). The film thickness was typically 10 unit cells (~ 4 nm). The substrates were annealed at 900 °C for 10 min at an oxygen pressure of 5×10^{-6} Torr to obtain an atomically flat step-and-terrace surface prior to film growth. The films were grown at 700 °C and 5×10^{-6} Torr of oxygen using a polycrystalline SrTi_{0.95}Ir_{0.05}O₃ target. The polycrystalline target was ablated with a KrF excimer laser ($\lambda = 248$ nm) at a laser fluence of ~ 0.64 J/cm² and a repetition rate of 1 Hz. The growth rate (~ 145 pulses/nm) was monitored in real time by reflection high-energy electron diffraction (RHEED). The film surface

morphology was characterized by ex situ AFM. Observation of the atomic-scale crystal structure along the (100) direction was performed on cross-sectional samples using high-angle annular dark-field scanning transmission electron microscopy (HAADF-STEM) with a spatial resolution of ~ 0.08 nm. The HAADF collection angle extended from 68 to 280 mrad, efficiently minimizing diffraction effects. Energy-dispersive X-ray (EDX) spectrometry was used to analyze the local chemical composition in the cross-sectional specimens. The STEM specimens were prepared by focused ion beam (FIB) microsampling, followed by thinning with 30 keV Ga ions. Finally, low-energy (5 keV) broad-beam milling was used to reduce FIB damage. The final thickness of the specimen was about 40 nm. The top surface of the film was protected by a conducting polycrystalline Pt layer, which can be observed in the displayed images. The Ir valence was determined by X-ray photoelectron spectroscopy (XPS) using an Al K α X-ray source (1486.6 eV).

First-principles calculations based on the density functional theory (DFT) were performed using the projector augmented-wave method¹³ as implemented in the Vienna ab initio simulation package^{14,15} and with a cutoff energy of 500 eV. The first Brillouin zone was sampled by a $6 \times 6 \times 1$ Monkhorst-Pack grid.¹⁶ The exchange-correlation energy was approximated by the generalized-gradient approximation (GGA-PBE) method.¹⁷ The atomic structure was optimized for a symmetric slab built with $3 \times 3 \times 6.5$ SrTiO₃ unit cells (u.c.) and delimited by TiO₂-terminated surfaces separated by a vacuum thickness of at least 1.5 nm. The lateral lattice parameters were fixed to the calculated value for SrTiO₃ ($a = 0.3947$ nm). Each structural model contains two Ir atoms substituting Ti atoms, as octahedral atomic sites were found to be the most favorable for such substitution.¹⁸

3. RESULTS AND DISCUSSION

Oscillations of the RHEED specular spot intensity observed during the deposition of an Ir:SrTiO₃ film are shown in Figure 1a. Clear oscillations can be observed for at least 10 u.c., which indicates that the growth proceeded in a layer-by-layer mode.¹⁹ However, the intensity of the oscillations clearly decreases. Because the film surface retains a step-and-terrace morphology, as shown by the AFM image in Figure 1b, we can conclude that the oscillation intensity drop is not associated with a spread of the crystal growth front over several unit cell layers but is instead related to the local surface roughness increase during the growth of an Ir-doped SrTiO₃ film.

An abrupt change in the intensity oscillations occurs after 300 s, at a film thickness of 6 u.c. This type of specular intensity phase shift has been associated with a change of the surface termination of the film.²⁰ Because the chemically etched substrate surface is initially terminated by the TiO₂ layer, we can assume that during the growth of the first five u.c., the film retains the perovskite B-site TiO₂ termination. Figure 1b shows the morphology of the film surface after the growth of four u.c. Clearly, the step-and-terrace surface morphology of the SrTiO₃ substrate was replicated on the film surface. Because the growth of nondoped SrTiO₃ proceeds under identical growth conditions in a layer-by-layer mode for hundreds of u.c.,²¹ the surface change observed in Ir-doped films thicker than 5 u.c. is most likely related to segregation of the Ir dopants.

Figure 2a shows a cross-sectional HAADF-STEM image of a 10 u.c. thick Ir:SrTiO₃ film taken along the [010] zone axis. The perfect match between the film and the substrate lattice, better observed in Figure 2b, shows that the film is fully epitaxial and coherent with the SrTiO₃ substrate. The images show several bright spots, about 1 nm in size, in the Ir-doped film. These bright spots are all located at the same depth from the surface within the first five u.c. of the film. Figure 2c presents an intensity profile of the atomically resolved HAADF image displayed in Figure 2b, integrated over a direction parallel to the interface. It shows that the presence of the bright spots causes a contrast blurring that does not affect the atomic plane spacing but increases the background intensity. Such bright spots are commonly observed in HAADF-STEM images when transverse atomic displacements occur, originating from strain fields associated with dislocation cores or point defects.²² In our case, the observed contrast is most probably caused by local enrichment with Ir atoms, favoring local structural distortions and, Ir being heavier than Ti, enhancing the Z-contrast (atomic number contrast) in the HAADF-STEM image.

The variation of the Ir concentration in different parts of the film was analyzed by acquiring EDX spectra in the square regions defined in the HAADF-STEM images shown in Figure 3. To distinguish the Ir L α peak at 9.174 keV, the figure presents magnified regions of the EDX spectra in an energy range close to the Cu K peaks, which originate from the copper grid on which the sample was mounted. Comparison of the spectra shows that the Ir L α peak has a much higher intensity in the bright spots (Figure 3a) than in the darker regions in which almost no Ir was detected (Figure 3b). A slight Ir enrichment is also observed in the vicinity of the film surface (Figure 3c,d). The evolution of the Ir peak intensity from the substrate toward the film surface is clearly observed in the line profile of the Ir L α peak amplitude recorded across a bright spot and displayed in Figure 3d.

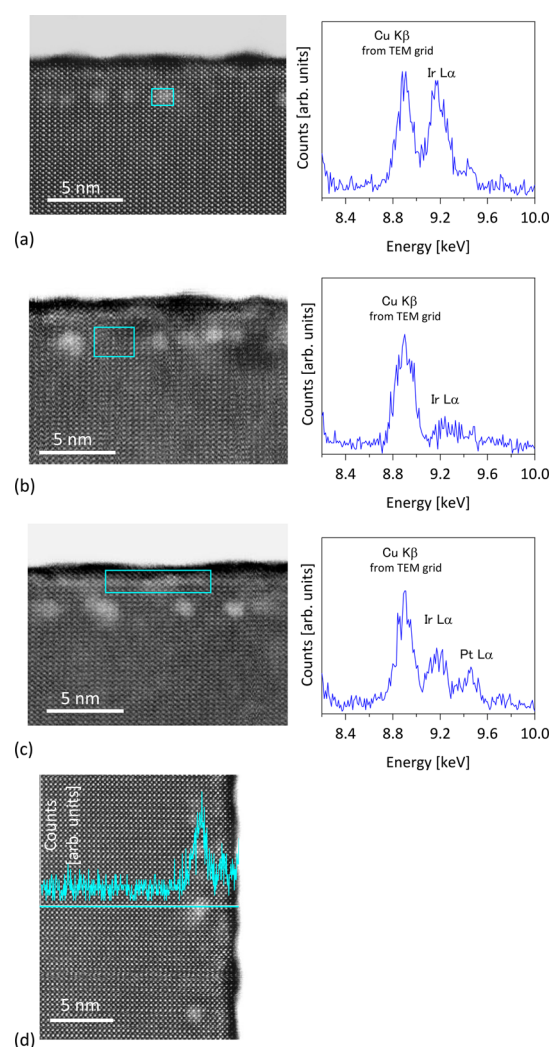


Figure 3. EDX spectra recorded at three different regions of the same 5% Ir-doped SrTiO₃ film giving evidence for a strong variation in the Ir content. (a) Ir L α peak measured at a bright spot, (b) Ir L α peak measured in between bright spots, (c) Ir L α peak measured close to the surface, and (d) line profile across a bright spot.

The bright spots are thus clearly associated with local Ir enrichment in regions that are 2–4 u.c. wide (about 0.8–1.5 nm). The bright spots appear to be well-separated, the projected distance between them being 2–8 nm for a ~40 nm thick cross-sectional specimen.

The relative stability of Ir cations as a function of substitution of Ti octahedral site location in the film was investigated by DFT calculations. Three configurations with different Ir distributions were considered: with one Ir atom in each TiO₂ surface layer (Figure 4 S), with one Ir atom in each TiO₂ subsurface layer (Figure 4 S-1), and with two Ir atoms in the same TiO₂ central atomic layer (Figure 4 C). The results show that for sufficiently low Ir doping levels, the positioning of the two Ir atoms at the surface (S) is energetically less stable by 0.59 eV than having the Ir atoms located in the subsurface layer (S-1) or in the center (C) of the slab. These two last configurations (S-1 and C) have the same stability as they give almost equal total energies with a difference of only 0.01 eV, confirming that, away from the surface, Ir atoms do not have any preferential location (far or near each other), as far as they

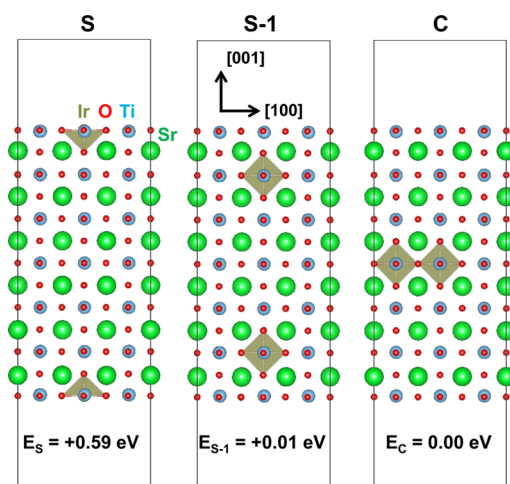


Figure 4. Atomic structures used for calculations, two Ir atoms in $3 \times 3 \times 6.5$ SrTiO₃ supercell ($\sim 3.2\%$ Ir): with one Ir atom in each TiO₂ surface layer (S), with one Ir atom in each TiO₂ subsurface layer (S-1), and with the two atoms in the same center TiO₂ atomic layer (C). The relative energetic stability of the different configurations is shown for each configuration. The total energy of the most stable structure (C) is taken as a reference.

are located in an octahedral atomic site. This result agrees with our previous calculations performed on Ir-doped bulk SrTiO₃.¹⁸

The nature of the iridium atoms within the film and close to the surface was investigated using XPS. XPS spectra of the Ir 4f_{5/2} and 4f_{7/2} core level peaks are shown in Figure 5. Deconvolution of the peak profile showed that the Ir:SrTiO₃ film contained Ir⁴⁺ and Ir⁰ components. The inelastic mean free path of photoelectrons in an XPS measurement using the Al K α source is only a few nanometers, which means that the depth distribution of the Ir⁴⁺ and Ir⁰ components can be estimated by measuring spectra at different takeoff angles. Measurements closer to the surface normal direction can detect photoelectron emission from deeper layers than measurements done at lower takeoff angles, which are more surface-sensitive. Figure 5a,b shows Ir 4f peak profiles measured at 45° and 20° takeoff angles (as measured from the sample surface), respectively. The Ir⁰ ratio ($\sim 13\%$) was higher in the more surface-sensitive spectrum taken at a takeoff angle of 20°. In comparison, the Ir⁰ ratio was $\sim 10\%$ for the 45° spectrum. Whereas trivalent Ir³⁺ is expected for iridium atoms substituted for Ti, as considered in the DFT calculations, metallic Ir⁰ is observed. The Ir⁰ content difference between the two takeoff angles is small, and

considering the effective probing depth, metallic Ir⁰ is likely to be present in the clusters observed by HAADF-STEM.

This result suggests that clustering and the appearance of metallic Ir⁰ already occurs for 5% doping and shows that the Ir dopant atoms are not homogeneously distributed among the Ti sites of the host SrTiO₃ lattice.

Ir is known to form macroscopic self-organized metallic nanopillars in SrTiO₃ when films are grown by PLD at intermediate oxygen pressures of around 1 mTorr.⁶ In the present study, the films were grown at 5×10^{-6} Torr, a pressure which was assumed to yield homogeneously doped Ir:SrTiO₃ films, where uniformly distributed Ir atoms occupy Ti sites of the SrTiO₃ lattice. However, whereas AFM images of the films showed no surface structures suggesting Ir segregation, atomically resolved HAADF-STEM images and associated EDX analyses gave evidence for the occurrence of segregation of the Ir atoms forming Ir-rich cluster in the films. A possible scenario can be derived from the obtained experimental results. The XPS spectra show that metallic Ir⁰ is present in the film, which means that Ir must occupy other lattice sites besides just replacing Ti. Because the films are grown at a low oxygen pressure of 5×10^{-6} Torr and oxygen vacancies thus exist in the lattice during growth, the most likely cluster formation scenario is the placement of Ir atoms at the oxygen site, forming a metallic defect in the crystal. It is known that under suitable thermodynamic and kinetic growth conditions, nanometer-scale fcc-type metallic Ir inclusions can form in Ir:SrTiO₃. Most likely, the clusters observed in the HAADF-STEM images in this work are the initial seeds of such macroscopic metal inclusions.

The Ir-rich cluster size appears to be quite uniform, and the distribution of clusters in the growth direction is clearly not random. There are a large number of clusters in the HAADF-STEM image within the first five u.c., but no clusters can be found in the next three u.c. of the film. Considering the phase shift observed in the RHEED intensity oscillations, it appears that the cluster formation and growth are related to the surface composition of the film and the lateral diffusion rate of Ir on the surface.

4. CONCLUSIONS

We have shown that Ir-rich clusters form in Ir-doped SrTiO₃ films during the initial growth phase. Although the formation of macroscopic Ir metallic inclusions in SrTiO₃ has been observed before,⁶ the STEM-EDX analysis in this work shows that Ir clustering occurs on a unit cell scale even when films are grown

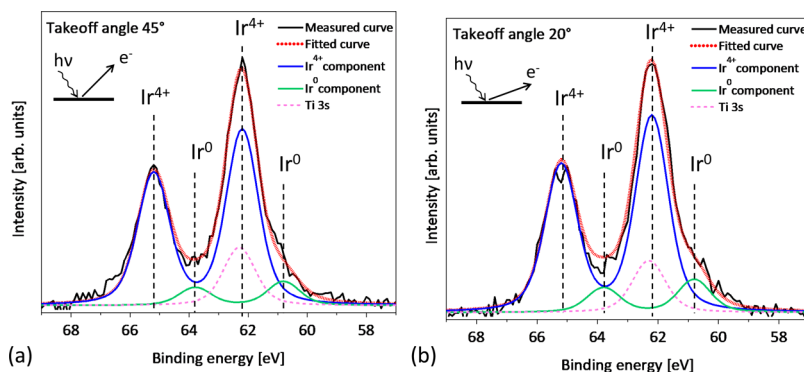


Figure 5. Ir 4f_{5/2} and 4f_{7/2} XPS spectra of a 5% Ir-doped SrTiO₃ film taken with an Al K α X-ray source (1486.6 eV). The takeoff angle from the sample surface was 45° in (a) and 20° in (b). The spectrum in (b) is more surface-sensitive.

at low oxygen pressures. Because the cluster size of 2–8 nm is below the AFM spatial resolution limit, such segregation is difficult to detect by surface morphology analysis. Even if no obvious surface segregation is seen by AFM, Ir clustering may still occur. We showed that the small clusters cannot be seen in surface topography but can be detected by STEM. This pointed out to the importance of combining topography analyses with XPS or STEM exploration to verify whether metal clustering occurs when synthesizing noble metal-doped perovskites for photo-electrochemical applications. The extent of the nanoclusters in the growth direction depends on a combination of thermodynamic (temperature and oxygen pressure) and kinetic (growth rate) factors. We find that the 5% doping level exceeds the solubility limit of homogeneous Ir:SrTiO₃ in SrTiO₃, as shown by the XPS measurement, excess Ir segregation starting immediately at the initial growth stage. The mechanism studied here is expected to be an effective method for synthesizing photoelectrode materials based on noble metal nanoclusters supported in an oxide matrix. The application area of such materials is photo-electrochemical energy conversion.

AUTHOR INFORMATION

Corresponding Authors

*E-mail: lee.mihee.ld7@ms.naist.jp (Mihee Lee).

*E-mail: mlippmaa@issp.u-tokyo.ac.jp (Mikk Lippmaa).

ORCID

Mihee Lee: 0000-0003-2351-164X

Ryota Takahashi: 0000-0003-2430-2444

Notes

The authors declare no competing financial interest.

ACKNOWLEDGMENTS

The work was partially supported by the NAIST Presidential Special Fund and by Grants-in-Aid for Scientific Research 26105002 and 17H04895 from the Japan Society for the Promotion of Science. This work was granted access to the HPC resources of CALMIP supercomputing center under the allocations p1313 and p1509 (2016–2017). The authors gratefully acknowledge Lucien Datas and Teresa Hungria for their assistance with the ARM200F at the UMS Castaing of Toulouse University and Robin Cours for his help with the TEM specimen preparation at CEMES.

REFERENCES

- (1) Ray, C.; Pal, T. Recent advances of metal–metal oxide nanocomposites and their tailored nanostructures in numerous catalytic applications. *J. Mater. Chem. A* **2017**, *5*, 9465–9487.
- (2) Liu, X.; Iocozzia, J.; Wang, Y.; Cui, X.; Chen, Y.; Zhao, S.; Li, Z.; Lin, Z. Noble metal–metal oxide nanohybrids with tailored nanostructures for efficient solar energy conversion, photocatalysis and environmental remediation. *Energy Environ. Sci.* **2017**, *10*, 402–434.
- (3) Munnik, P.; de Jongh, P. E.; de Jong, K. P. Recent Developments in the Synthesis of Supported Catalysts. *Chem. Rev.* **2015**, *115*, 6687–6718.
- (4) Shiraishi, Y.; Yasumoto, N.; Imai, J.; Sakamoto, H.; Tanaka, S.; Ichikawa, S.; Ohtani, B.; Hirai, T. Quantum tunneling injection of hot electrons in Au/TiO₂ plasmonic photocatalysts. *Nanoscale* **2017**, *9*, 8349–8361.
- (5) Wang, D.; Hisatomi, T.; Takata, T.; Pan, C.; Katayama, M.; Kubota, J.; Domen, K. Core/Shell Photocatalyst with Spatially Separated Co-Catalysts for Efficient Reduction and Oxidation of Water. *Angew. Chem., Int. Ed.* **2013**, *52*, 11252–11256.

- (6) Kawasaki, S.; Takahashi, R.; Yamamoto, T.; Kobayashi, M.; Kumigashira, H.; Yoshinobu, J.; Komori, F.; Kudo, A.; Lippmaa, M. Photoelectrochemical water splitting enhanced by self-assembled metal nanopillars embedded in an oxide semiconductor photoelectrode. *Nat. Commun.* **2016**, *7*, 11818.

- (7) Nishihata, Y.; Mizuki, J.; Akao, T.; Tanaka, H.; Uenishi, M.; Kimura, M.; Okamoto, T.; Hamada, N. Self-regeneration of a Pd-perovskite catalyst for automotive emissions control. *Nature* **2002**, *418*, 164–167.

- (8) Zhang, W.; Ramesh, R.; MacManus-Driscoll, J. L.; Wang, H. Multifunctional, self-assembled oxide nanocomposite thin films and devices. *MRS Bull.* **2015**, *40*, 736–745.

- (9) Zaera, F. Nanostructured materials for applications in heterogeneous catalysis. *Chem. Soc. Rev.* **2013**, *42*, 2746–2762.

- (10) Yoshida, M.; Takanabe, K.; Maeda, K.; Ishikawa, A.; Kubota, J.; Sakata, Y.; Ikezawa, Y.; Domen, K. Role and Function of Noble-Metal/Cr-Layer Core/Shell Structure Cocatalysts for Photocatalytic Overall Water Splitting Studied by Model Electrodes. *J. Phys. Chem. C* **2009**, *113*, 10151–10157.

- (11) Hou, X.; Takahashi, R.; Yamamoto, T.; Lippmaa, M. Microstructure analysis of IrO₂ thin films. *J. Cryst. Growth* **2017**, *462*, 24–28.

- (12) Kiss, B.; Manning, T. D.; Hesp, D.; Didier, C.; Taylor, A.; Pickup, D. M.; Chadwick, A. V.; Allison, H. E.; Dhanak, V. R.; Claridge, J. B.; Darwent, J. R.; Rosseinsky, M. J. Nano-structured rhodium doped SrTiO₃-Visible light activated photocatalyst for water decontamination. *Appl. Catal., B* **2017**, *206*, 547–555.

- (13) Blöchl, P. E. Projector augmented-wave method. *Phys. Rev. B: Condens. Matter Mater. Phys.* **1994**, *50*, 17953–17979.

- (14) Kresse, G.; Hafner, J. Ab initio molecular-dynamics simulation of the liquid-metal–amorphous-semiconductor transition in germanium. *Phys. Rev. B: Condens. Matter Mater. Phys.* **1994**, *49*, 14251–14269.

- (15) Kresse, G.; Furthmüller, J. Efficient iterative schemes for ab initio total-energy calculations using a plane-wave basis set. *Phys. Rev. B: Condens. Matter Mater. Phys.* **1996**, *54*, 11169–11186.

- (16) Monkhorst, H. J.; Pack, J. D. Special points for Brillouin-zone integrations. *Phys. Rev. B: Solid State* **1976**, *13*, 5188–5192.

- (17) Perdew, J. P.; Burke, K.; Ernzerhof, M. Generalized Gradient Approximation Made Simple. *Phys. Rev. Lett.* **1996**, *77*, 3865–3868.

- (18) Lee, M.; Arras, R.; Warot-Fonrose, B.; Hungria, T.; Lippmaa, M.; Daimon, H.; Casanove, M. J. Strain induced atomic structure at the Ir-doped LaAlO₃/SrTiO₃ interface. *Phys. Chem. Chem. Phys.* **2017**, *19*, 28676–28683.

- (19) Lippmaa, M.; Nakagawa, N.; Kawasaki, M.; Ohashi, S.; Koinuma, H. Growth mode mapping of SrTiO₃ epitaxy. *Appl. Phys. Lett.* **2000**, *76*, 2439–2441.

- (20) Matvejeff, M.; Chikyow, T.; Lippmaa, M. Interface growth of La_{1.2}Sr_{1.8}Mn_{1.7}Ru_{0.3}O₇ Ruddlesden–Popper films on SrTiO₃. *J. Cryst. Growth* **2009**, *311*, 1201–1205.

- (21) Ohnishi, T.; Shibuya, K.; Yamamoto, T.; Lippmaa, M. Defects and transport in complex oxide thin films. *J. Appl. Phys.* **2008**, *103*, 103703.

- (22) Muller, D. A.; Nakagawa, N.; Ohtomo, A.; Grazul, J. L.; Hwang, H. Y. Atomic-scale imaging of nanoengineered oxygen vacancy profiles in SrTiO₃. *Nature* **2004**, *430*, 657–661.